LU TP 19-13
June 2019

PARTON SHOWER UNCERTAINTIES ON THE TOP MASS

Hristina Hristova

Department of Astronomy and Theoretical Physics, Lund University

Bachelor thesis supervised by Torbjörn Sjöstrand

LUNDS
UNIVERSITET

Abstract

The non-Abelian QCD nature allows for pp collisions to contain gluon emissions off quarks as well as gluon branchings into further gluons — a structure that can be described by the parton shower model. In this project we present the results of the impact the shower has on the reconstruction of the W-boson and top quark masses using Pythia, the Lund Monte Carlo event generator. As a warm-up, the importance of showers and of multiparton interactions, as well as the value of the strong coupling constant, is investigated. We further study the results from different parton shower implementations by comparing the data of the default Pythia shower with the one from three other algorithms — the initial-state dipole recoil in Pythia, the dipole-like Dire and the antenna-based Vincia showers. Comparisons on reconstructed top masses are presented both for a common default α_S value and for one roughly tuned to give the same jet profile for all models. Unexpectedly large differences have been observed, amounting to $\pm 0.5\,\text{GeV}$ in some cases. More detailed research could either reveal the origin of these discrepancies, or conclude that there is still a long way to go until the value of the top mass can be safely extracted from data.

Populärvetenskaplig sammanfattning

Partikelfysikens standardmodell har framgångsrikt förutsagt de nu kända elementära partiklarna och deras växelverkningar. Liksom varje fysikmodell har den ett giltighetsområde. Det okända som kan tänkas inträffa utanför detta område kallas fysik bortom standardmodellen. Nya fenomen kan förväntas uppträda vid extremt höga energier, bortom de tillgängliga vid dagens kolliderare. En av de aspekter vi hoppas att en ny teori skulle ge oss förståelse för är topkvarkens extremt tunga massa. Denna massa svarar mot att Yukawakopplingen mellan top och Higgs är nära ett, och en så stor koppling spelar en betydelsefull roll i frågan om det elektrosvaga vacuumets stabilitet.

Studier av detta slag kräver hög experimentell precision vid mätning av topkvarkens massa. Olyckligtvis innehåller de händelser där top–antitop par bildas också mycket annan aktivitet som inte direkt är relaterat till den intressanta processen. Ett viktigt exempel är att kvarkar kan emittera gluoner som i sin tur kan splittras vidare, något som kan beskrivas i termer av s.k. partonkaskader. En annan svårighet är att kvarkar bär stark-växelverkan-färg och därför inte kan observeras direkt. Istället producerar de kollimerade partikelskurar, jets, som kan observeras i en detektor. Men man kan aldrig med säkerhet ange en individuell partikels ursprung. Det är därför viktigt att förstå hur dessa jets uppför sig, och för detta är experimentalister mycket beroende av händelsegeneratorer, där denna fysik modelleras. Ett sådant program, som användes i denna studie, är Pythia som huvudsakligen är skrivet av Lundafysiker.

Simuleringen av protonkrockar styrs enligt specifika modeller och algoritmer, som i sig innehåller ett mått av osäkerhet. I fokus av det nuvarande arbetet ligger en jämförelse mellan tre olika skuralgoritmer, nämligen Pythia, Dire och Vincia, varav de två sistnämnda kan användas inuti Pythia. Detta görs genom att generera semirealistiska proton-protonkollisioner som sedan analyseras på ett sätt som rimligt nära anknyter till vad som kan göras experimentellt. I analysen av tophändelser hittas jettarna och kombineras för att försöka rekonstruera W-bosonens och topkvarkens massor.

Våra första studier visar att bägge de rekonstruerade massorna varierar som väntat när den starka kopplingens värde varieras, eller när inga partonkaskader tillåtes, eller när kollisioner mellan ytterliggare partonpar i de inkommande protonerna inte tas med. Resultaten från de centrala studierna i detta arbete, med tre olika partonkaskader, var inte entydiga. De tydde ändå på att det — i brist på bättre förståelse av och kontroll över kaskaderna — finns en osäkerhet på ungefär ± 0.5 GeV i topkvarkens massa, jämförbar med den totala osäkerhet som ofta citeras vid LHC. Naturligtvis är vår studie fortfarande en förenklad version av den fulla experimentella, och i synnerhet har Dire och Vincia inte än utnyttjats till sin fulla potential.

Om vi summerar så är det imponerande att det faktiskt går att bestämma topmassan med så god precision, vilket visar på de stora framsteg som gjorts i vår förståelse av högenergikollisioner. Men det visar också på att vår förståelse har brister, att vi måste fortsätta sträva mot högsta möjliga precision. Man skall aldrig vara helt nöjd; det kommer alltid att finnas många fler vetenskapliga gåtor i behov av att redas ut.

Contents

Abbreviations

BSM - Beyond Standard Model

DGLAP - Dokshitzer–Gribov–Lipatov–Altarelli–Parisi

Dire - DIpole REsummation

FSR - Final-State Radiation

HO - Higher Order

IR - Infra-Red

ISR - Initial-State Radiation

LO - Leading Order

ME - Matrix Element

MPI - Multi-Parton Interaction

(N)NLO - (Next-to-)Next-to-Leading Order

PDF - Parton Distribution Function

QCD - Quantum ChromoDynamics

SM - Standard Model

Vincia - VIrtual Numerical Collider with Interleaved Antennae

1 Introduction

One of the most recent major successes in the field of particle physics came with the discovery of the Higgs boson at the Large Hadron Collider in 2012. This event marked the point at which all particles, that the Standard Model (SM) describes theoretically, are also confirmed experimentally. Ever since, physics beyond the SM (BSM) has been sought for. It has been argued [2] that, as of today, the only quantity that can give a sign about where the scale of new physics lies, is the top Yukawa coupling. With its extraordinarily heavy mass of approximately 173 GeV, the top quark couples the strongest to the Higgs boson compared to the rest of the fundamental particles, with a coupling approximately equal to unity. In higher order (HO) corrections, the large coupling contributes to the effective Higgs potential and thereby plays a significant role in the theory of vacuum stability. As of our current understanding, the borders between the meta-stable Universe we presumably live in, an absolute stable and an unstable one are extremely close. Therefore the top mass value influences the constraints on some scenarios of BSM physics, and a precise determination in turn requires a deep understanding of the perturbative and non-perturbative effects in a collision.

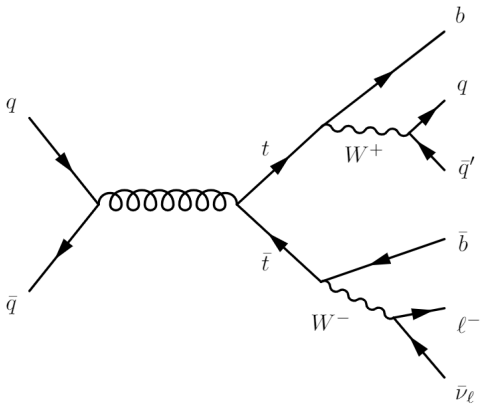

Figure 1: An example of the hard process of a pp event. The incoming $q\bar{q}$ pair can be substituted with a pair of gluons. The hadronic and leptonic decays of the two bosons can be interchanged. The Feynman diagrams are created using the *feynMP* package [1] in LaTeX.

The mass of the top quark has been measured with great accuracy and scientists keep striving for better results. It is determined up to less than a GeV, which, given its value, makes it the most precisely measured quark mass in terms of relative error. The task of performing such studies, however, is far from trivial. Color confinement allows us to observe only the color neutral products of a color triplet quark. Therefore, no one-to-one association of the original top quark and the final-state hadrons can be made. Experimentally, the "interesting" events, that have the signature of top–antitop production, need to be extracted out of millions of proton–proton collisions per second. Several different physics mechanisms disturb the simple picture of top production and decay, illustrated in Fig. 1, and to complicate background rejection.

A standard way to study the individual effects is with the help of event generators. These are tools which, using Monte Carlo methods [3], simulate the random nature of the microscopic world by generating a process given its quantum mechanical probability to occur. A large event sample needs to be generated in order to give the complete probability distribution of nontrivial observables. In a Monte Carlo generator, hadron collisions are calculated with leading order (LO) matrix element (ME), or potentially with higher orders.

The latter type of calculations increase rapidly in complexity, however. This points towards the need for an approximate perturbative model, e.g. in the form of *parton showers*. Since perturbation theory breaks down for large values of the coupling constant, hadronization cannot be calculated explicitly and needs to be modelled instead, together with other processes such as multi-parton interactions (MPI).

In the current simulations, an event begins with the collision of two protons at a center-of-mass energy of 8 TeV. One of the effects that gives rise to uncertainties in the top mass reconstruction, and the one we studied in this project, is gluon radiation off partons before and after the proton collision, namely initial- (ISR) and final-state radiation (FSR). Such a process can be described approximately by parton showers. As shown in the diagram, a $q\bar{q}$ or a gg pair collision produces a gluon, which then splits into a top and an antitop quark. Undesirable, yet unavoidable, is the effect of MPI — the possible interaction between other proton constituents within the event, which might produce additional particles, not related to the top quark production. Its impact will be briefly discussed. Some other sources of uncertainties, which will not be covered in the project, are pile-up events and color reconnection [4]. The first effect is the presence of particles belonging to other events than the top production one and is a result of the high luminosity that colliders obtain. The second one, constituting 20% to 40% of the uncertainty [4], occurs towards the end of an event, during hadronization, and is a consequence of the combined effects of parton showers and MPI. Colored $q\bar{q}$ and gg pairs form color dipoles, whose overlap creates a nontrivial and fairly complicated behaviour [5, 6]. This list of possible uncertainty sources is, of course, far from complete. Scientists continue to improve, test and create models in order to arrive at the best possible picture describing all processes that can occur in an event of this nature.

The present thesis is concentrated on the effects that parton showers have on the precision of top quark mass measurements. Events are reconstructed using the Pythia 8.2 event generator [7, 3]. Nowadays parton showers are normally described in terms of dipole showers, but especially when ISR is involved the choice is not trivial. Two different Pythia dipole-recoil options are therefore compared [8]. The default Pythia parton showering is juxtaposed with two more modern dipole-shower algorithms, namely Dire 2.003 [9, 10, 11] and Vincia 2.3 [12].

The report is organized as follows. A brief discussion regarding MEs is given in Sec. 2.1. The following Sec. 2.2 introduces the idea of parton and dipole showers, as well as the different types of gluon emission. In Sec. 3 a summary of the jet algorithm, used in the project, is given. The three top decay channels are discussed in Sec. 4. The flow of the program leading to reconstruction of W and top masses, together with the simulation results are thoroughly discussed in Sec. 5. Final remarks and ideas for further improvements in Sec. 6 conclude the thesis.

Throughout the report we will be using the natural units, where the fundamental constants c and $\hbar$ are set to unity.

2 Physics Overview

2.1 Matrix Elements

Hadron–hadron collisions are Quantum Chromodynamics (QCD)-dominated events rich in activity and complexity. Describing them requires the introduction of various concepts and models, and leads to lengthy equations even for LO calculations. Nevertheless, better theoretical precision is needed and obtained by calculating HO corrections in perturbation theory. Unfortunately, this description is not applicable to the complete momentum range of an event. In contrast with Quantum Electrodynamics (QED), the strong coupling constant of QCD increases rapidly at low momentum transfer scales. This makes perturbation theory break down in that region and approximate solutions become necessary.

As a starting point for fixed-order calculations, let us firstly present the parton distribution/density function (PDF). It is written in the form $f_a^A(x, Q^2)$, which, at LO, gives the probability of finding a parton of type a inside a proton A, carrying a fraction x of the proton momentum, probed at a (space-like virtuality) scale Q^2. A cross-section of the parton–parton interaction is then obtained by the convolution of the PDFs of both incoming protons, A and B, and the differential cross-section of the hard-scattering between partons a and b:

$$\sigma = \sum_{a,b} \iiint \mathrm{d}x_1 \, \mathrm{d}x_2 \, \mathrm{d}\Omega \, f_a^A(x_1, Q^2) \, f_b^B(x_2, Q^2) \, \frac{\mathrm{d}\hat{\sigma}_{ab}}{\mathrm{d}\Omega}, \tag{1}$$

where Ω is the phase space of the process and $\hat{\sigma}_{ab}$ is a function of the kinematics variables. The latter is proportional to the squared ME, $|\mathcal{M}_{a+b\to N}|^2$, where N is the final parton multiplicity.

Computing the MEs is certainly the correct approach to evaluate the perturbative aspects of an event. The complexity of the method sets limitations to how precise calculations can be, however. In the cases of real corrections, which result in high final parton multiplicities, setting up the MEs is a tedious, yet straightforward task. The limiting factor is that each HO requires ever further increased computer capacity. In the cases of virtual (HO loop) corrections, on the other hand, the MEs are extremely challenging to set up since it requires calculations in non-integer dimensions to isolate and cancel unphysical divergences. Processes of the type $q\bar{q} \to t\bar{t} + X$, $qg \to t\bar{t} + X$ and $gg \to t\bar{t} + X$ have been calculated up to NNLO [13, 14, 15]. We can therefore conclude that, given a $2 \to N$ process, the ME approach can be applied only for small values of N.

2.2 Parton Showers

2.2.1 Description

The difficulties arising when using MEs have inspired people to search for perturbative approximate solutions to HO Feynman diagrams. This type of solutions have been developed in the form of parton showers. Instead of computing all MEs involved in a

single event, different kinds of branchings are generated recursively, one additional parton at a time, according to their probabilities to occur [16]. Despite the approximate shower nature, the results turn out to be surprisingly accurate. They cannot be applied to non-perturbative regions, however, such as hadronization — a process which takes over once a minimal cutoff around the value of $1\,\mathrm{GeV}^2$ is reached [3].

An important concept in our discussion here is the notion of *virtuality*. As we know from basic kinematics, the squared four-momentum of a particle amounts to the square of its rest mass:

$$p^2 = E^2 - \mathbf{p}^2 = m_0^2. \tag{2}$$

This is not necessarily true, however, especially in the case of highly energetic collisions. A good definition of virtuality would give an intuitive measure of how hard a process is and one such definition is given by the difference in the two above mentioned quantities [16, 17]:

$$Q^2 = p^2 - m_0^2. \tag{3}$$

The hard process in Fig. 1 (which should be defined as the hardest one in the whole event) is evaluated by fixed-order perturbative calculations. The parton shower method is thereafter used when estimating the probabilities for further parton emissions primarily in the collinear and soft regions. These are situations of small virtuality (in the former region), or small energy of the emitted gluon (in the latter one). Therefore, the ME and shower approaches ought to be combined in order to produce the complete event. We can safely make the approximation of firstly isolating the hard process from the parton branchings and then, for virtuality scales below those covered by the MEs, gradually add parton showers to the event [17].

Parton showers are conveniently split into two types: ISR (space-like showers, where $Q^2 < 0$) and FSR (time-like showers, $Q^2 > 0$). As the names suggest, the former/latter type occurs before/after the hard process. An event described by Fig. 1 can contain both initial and final QCD radiation, both of which obey Heisenberg's uncertainty principle:

$$\Delta E\,\Delta t \sim \frac{\hbar}{2}, \tag{4}$$

where ΔE is the energy scale at which the radiation is probed and Δt is the time interval between the hard collision and the radiation. We can interpret ΔE as related to the virtuality scale which, for comparable emission energies, is related proportionally to the emission angles. This results in gluons radiated at wide angles closely before/after (for ISR/FSR) the hard process has occurred. Conversely, the longer the time interval, the more low-angle the radiated gluons are.

Throughout the discussion so far, it has been hinted that events are not described in terms of their evolution with time, but with their evolution in hardness instead. However, this choice of *evolution variable* is not necessarily obvious. Different Monte Carlo generators have taken different approaches, each having its pros and cons. In the latest Pythia versions, this parameter approximately corresponds to the transverse momentum, $p_\perp$, of

the particle [18], given by:

$$p_\perp^2 = z\,(1-z)\,Q^2 \qquad \text{for FSR,} \tag{5}$$
$$p_\perp^2 = (1-z)\,\left|Q^2\right| \qquad \text{for ISR,} \tag{6}$$

where the energy-sharing z parameter will be defined in the upcoming section. For ISR, the quarks are considered massless, therefore the term m_0^2 in eq. (3) is omitted. It is clear that we cannot make this approximation for FSR due to the non-negligible masses of the top and the bottom quarks.

2.2.2 Final-State Radiation

Let us first study the more intuitive approach used in FSR calculations, whereby the hard process sets the beginning of the evolution. This method is called a *forward evolution* since the radiation is studied forward in time and the energy of a parton decreases with each emission.

Consider a branching of the form $a \to bc$, which can occur in either of the three forms (Fig. 2):

$$q \to qg \qquad g \to gg \qquad g \to q\bar{q}. \tag{7}$$

The virtuality of the cascade initiator a is given as Q^2. For the time being, we further assume that the final partons of the branching are massless (which should, in general, be corrected for) and on-shell. A variable z is then defined as the fraction of the initial parton energy that b carries:

$$z = \frac{E_b}{E_a} \qquad 1 - z = \frac{E_c}{E_a}. \tag{8}$$

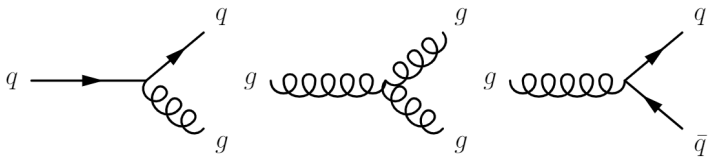

Figure 2: The three types of QCD branching processes.

In the heart of the parton shower technique is the probability for a certain branching to take place. The three types of branchings from eq. (7) are described by the *Altarelli-Parisi splitting functions* (or splitting kernels) [19]:

$$\hat{P}_{q\to qg}(z) = C_F\,\frac{1+z^2}{1-z} \tag{9}$$
$$\hat{P}_{g\to gg}(z) = C_A\left[\frac{1-z}{z} + \frac{z}{1-z} + z\,(1-z)\right] \tag{10}$$
$$\hat{P}_{g\to q\bar{q}}(z) = T_R\left[z^2 + (1-z)^2\right], \tag{11}$$

where the three constant color factors are

$$C_F = \frac{4}{3} \qquad C_A = 3 \qquad T_R = \frac{1}{2} \tag{12}$$

and eq. (9) bears the same form if the quarks are replaced by antiquarks. These equations are related to the probability for parton a to branch into two other, b and c, given the energy share z. Showers are evaluated at LO, for which the expressions bear the same form for both FSR and ISR. The (naïve) probability expression is then proportional to the kernels [17, 16]:

$$\mathrm{d}\mathcal{P}^{\text{naïve}}_{a\to bc} = \frac{\alpha_S}{2\pi}\frac{\mathrm{d}Q^2}{Q^2}\,\hat{P}_{a\to bc}(z)dz. \tag{13}$$

The term $\dfrac{1}{Q^2}$ is referred to as the collinear/mass singularity and $\dfrac{1}{1-z}$ is called the soft-gluon/IR singularity (which is symmetric to the $\dfrac{1}{z}$ singularity). The relation gives the probability for a branching (the one described by the splitting function) to occur between virtualities $Q^2 + \mathrm{d}Q^2$ and Q^2. We can read from eq. (13) that, as the event evolves towards lower virtuality, the splitting probability becomes larger and the parton multiplicity increases more rapidly.

2.2.3 The Sudakov Form Factor

The discussion so far faces an unpleasant problem. The probability from eq. (13) is prone to give results exceeding unity when integrated over large Q^2 regions. What has been falsely allowed is that, after the decay of parton a in the form $a \to bc$, it can yet again decay to, say, $a \to de$. This requires the introduction of an additional term, which gives the probability expression a physical meaning. A process that encompasses the same issue is nuclear decay, where a given nucleus should be allowed to decay only once (a thorough discussion is given in [17]).

A solution comes in the form of the *Sudakov (form) factor*, which, for FSR, is defined by the following, seemingly complicated, expression:

$$\Delta_{\text{FSR}}(Q^2) \equiv \exp\left(-\sum_{b,c}\int_{Q^2}^{Q^2_{\max}}\frac{\mathrm{d}Q'^2}{Q'^2}\int_{z_{\min}(Q'^2)}^{z_{\max}(Q'^2)}\frac{\alpha_S}{2\pi}\,\hat{P}_{a\to bc}(z')\,dz'\right) = \tag{14}$$

$$= \exp\left(-\sum_{b,c}\int \mathrm{d}\mathcal{P}^{\text{naïve}}_{a\to bc}\right). \tag{15}$$

Here, we have primed the quantities under the integral, so that they are distinguished as integration variables. The limits of the second integral are determined by the kinematics of the specific branching [16]. This definition gives the probability for a branching, described by the splitting kernel, *not* to take place between $Q^2_{\max}$ and Q^2. It is constructed as the exponential function of the probability for the branching to occur. The negative sign in

front then sets the Δ_{FSR} function to run between 0 and 1. The naïve probability from eq. (13) is then combined with the Sudakov factor from eq. (15) to give the physical branching probability:

$$\mathrm{d}\mathcal{P}_{a\to bc} = \mathrm{d}\mathcal{P}^{\mathrm{naïve}}_{a\to bc} \exp\left(-\sum_{b,c}\int \mathrm{d}\mathcal{P}^{\mathrm{naïve}}_{a\to bc}\right). \tag{16}$$

Expressed in a more explicit form, the equation reads:

$$\mathrm{d}\mathcal{P}_{a\to bc} = \frac{\alpha_S}{2\pi}\frac{\mathrm{d}Q^2}{Q^2}\,\hat{P}_{a\to bc}(z)\,\mathrm{d}z\,\Delta_{\mathrm{FSR}}(Q^2). \tag{17}$$

It is now easy to see that the total branching probability can never exceed unity. Furthermore, if $Q^2_{\mathrm{max}} \gg Q^2$ then $\Delta(Q^2) \to 0$, which is reasonable, since it becomes more and more unlikely for a branching not to take place in a broader and broader region [20].

While, this way, the emission rate of a is restricted, it should be remembered that, once a has branched, the partons b and c created in the process are allowed to branch in their turn, from the scale of the $a \to bc$ downwards. Hence an ordered cascade may develop.

2.2.4 Initial-State Radiation

The effect of ISR is a bit more tricky to tackle, given the complicated structure of a proton as a "cloud of quasireal partons" [21]. The hard process in the event is a result of the collision between two partons, each originating from its corresponding incoming proton. Various issues arise when trying to describe ISR using the forwards-in-time evolution from FSR. Problematic is the fact that it cannot be predicted, from the beginning, which one of the proton constituents will participate in the collision, unless numerous trial-and-error procedures are executed, which becomes highly inefficient [21, 16]. A good approach is instead to start our ISR study from the desired hard process, and then evolve backwards in time, calculating the probability for a given parton to have originated from a particular branching [21]. This technique turns out to be a successful one and results in faster algorithms.

In order to describe the content of the hadrons, we recall the PDF functions given in Sec. 2.1. The quantity $f_b(x, Q^2)\,dx$ then provides the number of partons of species b with momentum fraction between x and dx, probed at a virtuality scale Q^2 [16]. The function $f_b(x, Q^2)$ cannot be determined theoretically, however its virtuality evolution is calculated perturbatively through the DGLAP equation:

$$\mathrm{d}f_b(x,Q^2) = \frac{\alpha_S}{2\pi}\frac{\mathrm{d}Q^2}{Q^2}\sum_a \int_x^1 \frac{\mathrm{d}x'}{x'}\hat{P}_{a\to bc}\left(z=\frac{x}{x'}\right) f_a(x',Q^2) \tag{18}$$

The probability evolution equation for this process looks slightly differently from what we have encountered in eq. (13):

$$\mathrm{d}\mathcal{P}^{\mathrm{naïve}}_{a\to bc} = \frac{\mathrm{d}f_b(x,Q^2)}{f_b(x,Q^2)} \tag{19}$$

What eq. (18) tells us is, knowing the distribution of the mother parton a at a given virtuality scale Q^2, how the distribution of the daughter parton b changes from Q^2 to $Q^2 + \mathrm{d}Q^2$. As usual, the process is described by the splitting function $\hat{P}_{a\to bc}$. The energy fraction z is defined as the momentum x that parton b carries over the momentum x' of particle a, where the latter runs between the integration limits x and 1. The expression from eq. (19) then gives a *conditional probability*: given a parton b at a virtuality scale $Q^2 + \mathrm{d}Q^2$, what the probability is that it was created by the branching $a \to bc$ in the range between Q^2 and $Q^2 + \mathrm{d}Q^2$ [17]. The equation is modified by a Sudakov factor, related to the above branching rate, in the spirit of eq. (16).

2.3 Dipole Showers in Pythia, Dire and Vincia

So far, we have been discussing $1 \to 2$ gluon emissions and branchings. Another approach has also been formulated in the form of the $2 \to 3$ gluon emissions off *color dipoles* [22, 23]. It can be understood by considering a pair of color–anticolor quarks, in the $N_C \to \infty$ limit [24], forming a color dipole/antenna. In this configuration, the emission of a gluon is viewed as the joint action of the quark and antiquark. As a simplification, used in some dipole algorithms but not in all, one of the two is designated as the radiator and the other as recoiler, where the former then is more strongly affected by the emission than the latter.

As an example, let us consider the branching $q_r \to q_b + g_{r\bar{b}}$ (with r and b denoting the colors), which takes the form $q_r + q_{\bar{r}} \to q_b + q_{\bar{r}} + g_{r\bar{b}}$ in the color dipole shower formalism. We call the two partons to the left of the arrow pre-branching, while the three ones to the right are post-branching. Initially, the formation of a color dipole requires an antired antiquark. After the emission of the gluon, color strings are stretched between the antired–red and antiblue–blue colors. Now the system therefore consists of two dipoles, each of which can radiate further in the next step. Dipoles can be formed in the initial (II) and final (FF) states separately. Dipoles can also be created between a particle in the initial and a particle in the final state (IF or FI, depending on which is the radiator and which the recoiler) [18].

The first shower to adopt this idea is the Ariadne Monte Carlo [23, 25]. Ever since, different dipole shower algorithms have been implemented, each following a unique philosophy. In this project, three algorithms based on color dipoles are studied, namely the one in Pythia, the dipole-like Dire and the antenna-based Vincia. The main distinctions between the showers consist of the different definitions of kinematics, splitting and evolution variables, as well as splitting kernels.

In the default Pythia algorithm, the approach is to evolve events in transverse momentum using eq. (6). The ISR is handled via the *global recoil* scheme, where only II dipoles are created and the recoil is taken by the non-emitting parton in the initial state. The invariant mass of the system remains unchanged and thus the whole final state is boosted in the transverse direction [16]. The splitting variable z is defined as the energy sharing in the rest frame of the process, more specifically the ratio between the squared invariant masses of the daughter+recoiler and mother+recoiler. Shower evolution is strictly ordered,

starting from the highest $p_\perp$ and evolving backwards, thereby preventing double-counting a hard emission. This leads to some potential problems, however, such as leaving a "dead zone", where the phase space for high $p_\perp$ emissions is not populated. One solution is introducing the so-called "smooth ordering" applied in VINCIA [12].

This global recoil model is compared with a second PYTHIA algorithm, namely the *dipole recoil* ("DR = on") one. The difference is that IF color dipoles can form (depending on the process), where only one color-matched final-state parton takes the recoil of an ISR emission.

In contrast, the two other algorithms we will be working with consider pre-branching partons as a single color dipole object. Once an emission occurs, no distinction is made between a radiator and a recoiler in VINCIA, and only a modest such in DIRE. This "democratic" approach is achieved by introducing a modification of the $p_\perp$ evolution compared to the one mentioned above. In DIRE, it is given by the "soft" transverse momentum, defined as the $p_\perp$ of the two final dipoles in the center-of-mass frame of the decaying dipole. What makes the variable so attractive to use that it allows for filling the entire final-state phase space [9]. This change in evolution results in modified splitting kernels. The approach is then to keep the kernels fixed for II, FF, FI, IF at the expense of changing the energy sharing variable. Another DIRE specific component is the introduction of analytical weights [26]. Their construction is based on the Sudakov veto algorithm [27, 28] by defining an additional overestimate. The weight can then be calculated analytically rather than using the hit-or-miss method. The price to pay is that events come with variable weights, and even with negative-sign ones, requiring more careful bookkeeping.

In VINCIA there are two cases considered. By plugging eqs. (9), (10) and (11) into the probability from eq. (13) and taking the limit $z \to 1$, we note the following. The singularities in the first two cases restore the evolution variables from eqs. (5) and (6), whereas the only singularity in the third case is the virtuality of the emission. Therefore, branchings of the form $q \to qg$ and $g \to gg$ evolve inversely proportional to the leading poles, while $g \to q\bar{q}$ evolves in virtuality. The VINCIA algorithm is constructed in the following way. For each of the three cases, II, FF and IF+FI, a different splitting kernel (antenna function) is defined, whereas the definition of the integration variables (singular limits) in the evolution equations is kept the same. In this respect, VINCIA distinguishes between "global" and "sector" antennae [29], where the former is applied in the version of the algorithm used for this study. The events in the VINCIA shower always come with a weight of unity. As a final remark, it should be noted that both DIRE and VINCIA obey the well-known DGLAP equations in the collinear limit.

2.4 Multi-Parton Interaction

Another process of interest, occurring during the collision, is multi-parton interaction, referred also as multiple interaction/scattering. This effect is a consequence of the rich internal structure of protons, namely three valence quarks, plus many sea quarks and gluons. As we discussed in Sec. 1, the production of a $t\bar{t}$ pair is obtained through the collision of a gluon or a $q\bar{q}$ pair. However, other parton pairs can also happen to interact,

giving rise to additional soft (or hard) QCD interactions. These interactions can affect the color flow and subsequently the final-state multiplicity in the event [30]. We will later show what consequences this effect has on the reconstructed top mass.

2.5 Hadronization

The final process of hadronization, that we will discuss briefly in this section, occurs towards the end of an event, at energies below the IR cutoff scale of $\sim 1\,\mathrm{GeV}^2$ where perturbation theory can no longer describe the behaviour of the partons. It consists of the formation of color-neutral final-state observable hadrons, which comes as a consequence of the color confinement in the theory of QCD. Several models have been proposed throughout the years, the most well-known of which are the cluster [31] and the string fragmentation models, where the second one has been described by the notable Lund string model [32, 33, 34, 35], which is at the core of the PYTHIA implementation.

The simplest example of a string is the one stretched between an original quark and antiquark on their way apart from each other, and can be viewed as a non-perturbative analogoue of the perturbative dipole already discussed. The tension in the string is constant, $1\,\mathrm{GeV/fm}$, meaning its energy is proportional to its length. There comes a point when the energy stored in the string is sufficient for the spontaneous production of another $q\bar{q}$ pair. This breaks the original string into two lower-mass subsystems, which may break further to ultimately produce the primary hadrons, some of which are unstable and decay further. In the case of strings stretched between $q - g - \bar{q}$, similarly to the color dipoles we discussed in Sec. 2.3 where the gluon enters as a kink in the string, the force on the gluon doubles compared to the simple $q\bar{q}$ picture due to the presence of two, instead of one, strings attached to it. This implies a higher hadron production rate in the region close to the direction of the gluon, compared to the case of only two quarks present. The model can be described using the idea of infinitely many colors in QCD, borrowing the colors already assigned to the partons during the FSR to define how string pieces will be stretched between the outgoing partons.

3 Jet Finding

The following section is greatly inspired by Refs. [36] and [37], where different types of jet algorithms, as well as their shortcomings, are described. The authors also examine jets closely and provide a description of their properties.

As mentioned before, due to color confinement, the quarks from a hadron–hadron collision cannot be observed independently. They instead hadronize to produce "collimated sprays of energetic hadrons", given the name *jets*. An essential factor for obtaining accurate results is the use of a reliable jet algorithm. What here is meant by *reliable*, are the following aspects [38]:

1. collinear safe — the collinear splitting of a parton should not alter the number of jets in an event;

2. IR safe — the emission of a soft parton should not act as a new seed for the formation of a stable jet;

3. facilitating experimental corrections for "noise", such as MPI and pile-up events;

4. small computing time, which requires efficient algorithms.

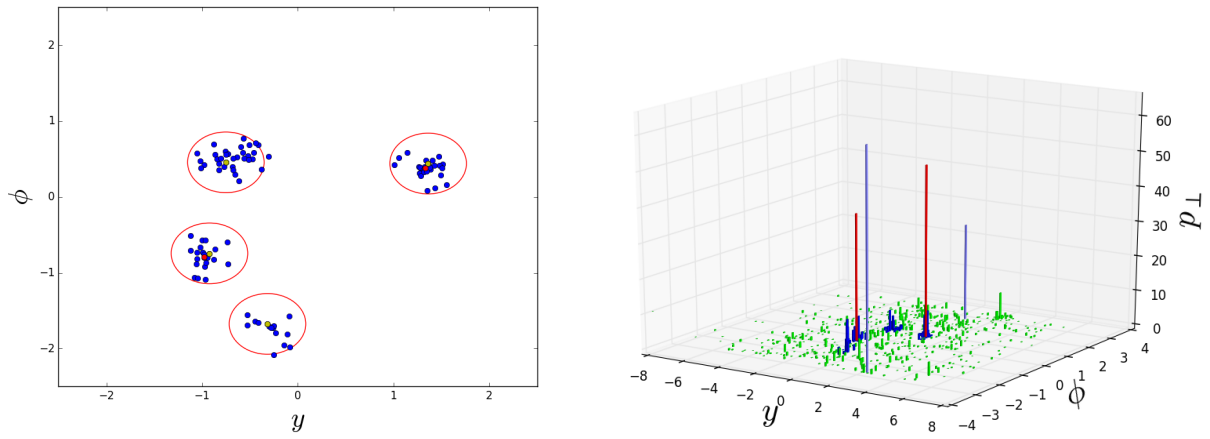

(a) (b)

Figure 3: Event with four reconstructed jets. In (a), the jets are plotted on the 2D $y - \phi$ plane. The jet constituents are colored in blue. The red dots among them show the location of the b-hadrons. The circles have radius 0.4 and each is centered at the hardest particle in the cluster. In (b), the figure from (a) is extended to a 3D view, where the height of the bars represents the particle transverse momentum and the color-code is kept the same. The light blue bars are the two leptons originating from the W, where the higher one designates the neutrino. The green bars show all final-state particles in the event. The plots are created using the *matplotlib* package [39] in *Python*.

For the "$k_\perp$ family" of jet algorithms, a jet cone radius R is chosen, where a typical choice would be 0.4 [40]. Below 0.4, the jets would include too few particles and the mass of the top quark would be underestimated. On the contrary, a jet with a larger radius suffers from enclosing particles that do not necessarily belong to the hadronization process of the top and would result in an overestimation. Although this is a safe choice when simulating events, the reasons for the small radius value are mainly experimental since high luminosity collisions suffer from higher production of pile-up events. Two counterarguments can enter here. The first one is that we have not accounted for this effect in the current simulations. Secondly, for $R = 0.5$ and 0.6, the number of events that contribute to the reconstruction of the top mass is higher than that for $R = 0.4$ and are seemingly a better choice. Nevertheless, the radius chosen is the one most frequently used in this type of top experiments using this particular jet algorithm.

Let us look more closely into how the algorithm is constructed. The radial separation between two particles (or pseudojets) i and j is determined in two dimensions, the variables being the difference in their rapidity, Δy_{ij}, and the difference in their azimuthal angle, $\Delta\phi_{ij}$:

$$\Delta R_{ij}^2 = \Delta y_{ij}^2 + \Delta\phi_{ij}^2 \tag{20}$$

Next, the distance between i and j, having transverse momenta $k_{\perp i}$ and $k_{\perp j}$, is defined as:

$$d_{ij} = \min\left(k_{\perp i}^{2p},\, k_{\perp j}^{2p}\right) \frac{\Delta R_{ij}^2}{R^2} \tag{21}$$

One more quantity is introduced further, namely the distance between i and the beams B:

$$d_{iB} = k_{\perp i}^{2p}. \tag{22}$$

Three types of algorithms have been developed depending on the value of p in eq. (21) and (22). The one used in this study is the anti-$k_\perp$ jet clustering algorithm, which is obtained by setting $p = -1$. Since we take the reciprocal of $k_{\perp i}^2$ (assuming $k_{\perp i}^2 > k_{\perp j}^2$), the distance between two particles is determined by the square inverse of the higher transverse momentum. The algorithm then returns smaller distances between a hard and a soft particle (or larger distances between two soft particles), favoring clustering around hard particles and minimizing the impact of soft QCD radiation. The clustering is performed iteratively, in each step joining the two objects with lowest d and thereby reducing their number by one. If $d_{iB} < d_{ij}$, then i is accepted as a jet (if its $k_\perp$ is above some threshold) and removed from further clustering. An example of jet reconstruction is shown on Fig. 3.

4 Top Quark Decay

Referring back to Fig. 1, the top quark decays weakly into a W^+ boson and (almost always) a b quark (and correspondingly for antiparticles). The values of the top–down and top–strange transitions in the Cabibbo-Kobayashi-Maskawa (CKM) matrix, being 3 orders of magnitude smaller than that for the the top–bottom decays, can be safely neglected. The decay width for this process and the lifetime of the top are given by [41]:

$$\Gamma_t(t \to bW^+) = \frac{G_F\, m_t^3}{8\sqrt{2}\,\pi} \left(1 - \frac{m_W^2}{m_t^2}\right)^2 \left(1 + \frac{2m_W^2}{m_t^2}\right) \tag{23}$$

where G_F is the Fermi constant, $m_t \approx 173\,\text{GeV}$ is the top mass and $m_W \approx 80.4\,\text{GeV}$ is the mass of the W [42]. Given those values, the width of the process is estimated to be $\Gamma_t \sim 1.5\,\text{GeV}$. The lifetime of the quark ($\tau_t = 1/\Gamma_t$) amounts to $\tau_t \sim 4 \times 10^{-25}\text{s}$ ($\sim 0.1\,\text{fm}$) — too short-lived to form bound states.

The decay possibilities for the W-boson are either $q\bar{q}$ pair, or a $\ell\bar{\nu}_\ell$ pair from the first two families[1]. The partial decay width of either process is given by:

$$\Gamma_W = \frac{\alpha_2 m_W}{12}, \tag{24}$$

[1]The τ lepton is omitted from the analysis as it raises further complications. It might decay to another lepton and two neutrinos, or a pion and a neutrino, which further increases the missing momentum in the event.

where α_2 is a coupling constant. Seemingly, the decay rate to quarks and leptons is the same. However, each $q\bar{q}$ pair can come in three different colors. Thus, the probability of decaying into quarks grows noticeably. Taking all these facts into account, let us look at the three different top decay channels.

Firstly, we will discuss the hadronic channel, where both Ws produce a $q\bar{q}$ pair. Following the above discussion, the channel has the highest branching ratio compared to the other two. What is more, all four-momenta is present since there are no neutrinos among the decay products. The channel has also some disadvantages, however, which cannot be neglected. In the ideal unrealistic situation of no ISR, FSR and MPI, we expect to find six jets at the end of the event, without any gluon emissions disturbing the measurements. Going back to reality, the aforementioned effects can give rise to additional jets and smear the properties of the ones from the bottom and W decay. A serious experimental issue is combinatorial background. Jets which do not belong to the top event of interest might be mistakenly taken into account. Therefore, numerous jet combinations should be tested, which further increases the task and the final errors. Moreover, without the advantage of a lepton (and neutrino) signal, top events will also be more difficult to distinguish from the background of QCD multijet events. These arguments restrain us from using the channel for our study.

The leptonic channel, as the name suggests, is the one where the W-bosons decay into a $\ell^-\bar{\nu}_\ell$ and a $\ell^+\nu_\ell$ pair. Here two jets are expected, coming from the b and the $\bar{b}$ quarks. Due to the large mass of the top quark, the outgoing leptons are highly energetic and stand out in the energy deposition of the detector. What is more, the two neutrinos, invisible for the detector, give rise to a missing transverse momentum. These two facts make the signature of the event easily recognizable but also explain the problem with using this decay channel: due to the missing momentum, we cannot determine the mass of the W accurately, and subsequently, also not the mass of the top.

Finally, in the semi-leptonic type of decay, one of the W-bosons produces a $q\bar{q}$ pair, whereas the other one gives a $\ell\nu_\ell$ pair. In the final state, we should observe a highly energetic lepton, a missing neutrino transverse momentum, as well as four jets (in most of the cases), coming from the $b\bar{b}$ and $q\bar{q}$. This is the most appropriate channel to use in our study, as it combines one top decay that stands out with one that allows mass reconstruction.

5 Results and Discussion

The following section is dedicated to giving a step-by-step description of how the W and top mass reconstruction has been performed and presenting the analysis. We will study what differences occur when the value of the strong coupling value is varied, how ISR, FSR and MPI affect the final results, and finally, the behaviour of different shower algorithms.

5.1 Program Flow

The analysis begins by running PYTHIA with the default shower options using three different α_S values for the time-like and space-like showers — 0.1365 (the default one), 0.1200 and 0.1500. The statistics is based on 2 million initial events, where half of them are generated with a hadronic W^+ decay and the other half with a hadronic W^- decay. The methodology is greatly inspired by Ref. [4].

- **Transverse momentum of the lepton** (all events)

  As mentioned in Sec. 4, the big mass of the top results, in most of the cases, in a highly energetic isolated lepton. The event is discarded if it happens to be one of the rare cases where the lepton transverse momentum $p_\perp$ is below 25 GeV. The plot on Fig. 4a shows the normalized $p_\perp$ distribution for the three α_S cases. It comes as no surprise that the curves overlap almost perfectly, since this parameter is barely affected by the strength of the strong coupling. The dashed line separates the surviving events from the removed ones. In this case, the events considered further are to the right of the line.

- **Pseudorapidity of the lepton** ($p_\perp > 25\,\text{GeV}$)

  In the relativistic limits, the values of the rapidity, y, and pseudorapidity, η, are sufficiently close:

  $$y = \frac{1}{2}\ln\left(\frac{E+p_z}{E-p_z}\right) \qquad \eta = -\ln\left(\tan\frac{\theta}{2}\right) \tag{25}$$

  The latter is preferred by experimental physicists due to its dependence on the angle θ between the beam axis and the emitted lepton. It is a more easily measurable quantity than the energy and momentum present in the rapidity equation.

  In an experimental environment, decay products emitted very close to the beam axis will not be caught by the detector. A maximal rapidity value should then be introduced, which we have chosen to be $|\eta| = 2.5$. This would mean that an event will be discarded if a lepton is emitted at an angle below $\approx 10°$.

  The histograms on Fig. 4b are constructed with the events satisfying the condition of the preceding section. We notice again the overlap of the curves and the great number of surviving events to the left of the dashed line.

  The algorithm needs to prevent the formation of a false jet around the particle. The lepton is therefore removed from consideration in the following steps.

- **Jet multiplicity** ($p_\perp > 25\,\text{GeV}$, $|\eta| < 2.5$)

  With the surviving set of events, jets are reconstructed using the anti-$k_\perp$ jet algorithm described in Sec. 3. The criteria by which jets are formed are listed below.

  1. Jet cone radius: $R = 0.4$;

2. Jet transverse momentum: $p_{\perp\text{jet}} > 25\,\text{GeV}$;
3. Detector pseudorapidity coverage: $|\eta|_{\text{jet}} < 2.5$;
4. Only visible final-state particles are considered, thus excluding neutrinos and other particles without strong or electromagnetic interaction;
5. The decay products of an event consist mainly of pions and photons. What is more, a detector is very often blind to the type of hadrons that have been produced. Therefore, in order for our model to be as close to an experimental environment as possible, a reasonable approximation is to set the mass of the neutral particles to be zero and the mass of the charged ones to the $\pi^{\pm}$ meson mass.

There are a couple of interesting conclusions that can be extracted from Fig. 4c. A higher α_S implies a higher rate of ISR/FSR and a larger final-state particle multiplicity. Therefore, we notice an increase in the five-, six- and seven-jet cases at the expense of lower multiplicities for the highest coupling value. Nevertheless, the events with exactly four jets have the highest rate for all three couplings.

Events with jet multiplicity bigger than or equal to 4 (to the right of the line) are considered further in the analysis, but only the first four hardest ones are used for the reconstruction of the W and top masses.

- **b-jet multiplicity** ($p_\perp > 25\,\text{GeV}$, $|\eta| < 2.5$, $n_{\text{jet}} \geq 4$)

  Next, we find the number of the most common b-hadrons that each event contains: $B^0, B^{\pm}, B_s^0$ and Λ_b^0. Their rapidity and azimuthal angle is retrieved. These parameters are plugged into eq. (20) in order to find which jets (called the b-jets) the hadrons belong to. As we discussed before, theoretically the event is expected to have exactly two b-jets. If any of the hadrons are found to belong to softer jets, then they are not considered as b-jets and will not contribute to the top mass reconstruction.

  The results can be seen on Fig. 4d. As predicted, most of the events fall into the category of having two hard b-jets. It should be noticed, however, that there are quite a few single b-jet events and more precisely, they become more as the strong coupling increases. A possibility of why this happens is the effect of ISR. The probability for the hard process initiators to radiate a gluon becomes larger for higher couplings. A highly energetic parton, that has been emitted right before the collision, might enter the event and create a jet of its own. If it happens to be more energetic than any of the b-jets, then the latter might end up in the "soft jets" category. This effect distorts the precision of the top mass reconstruction.

- **Reconstructed W mass** ($p_\perp > 25\,\text{GeV}$, $|\eta| < 2.5$, $n_{\text{jet}} \geq 4$, $n_b = 2$)

  So far, what is left to work with are the four hardest jets in the event — two b-jets from the decay of the bottom quark and two non-b-jets from the hadronic decay of one of the W-bosons. For the reconstruction of the W mass, the following is done:

1. the four-momentum sum, p, of the constituents of the two non-b-jets is calculated;
2. the invariant mass is obtained by:

$$m_W = \sqrt{p^2} = \sqrt{E^2 - |\mathbf{p}|^2}. \tag{26}$$

The familiar Breit-Wigner shape can be seen on Fig. 4e. Nearly half of the events are lost once we introduce the constraint of allowed W mass between 60 and 90 GeV (Table 1, rows 6 and 7). From the figure, it is seen that there is a positive shift (towards higher values) for smaller coupling constants (an effect that is also observed for the top mass distribution and will be discussed below). However, the first values in Table 2 show exactly the opposite type of behaviour, which might stem from the broad limits of plot. The values in the second row differ significantly from the previous one, this time following the decrease in mass with the increase in coupling.

A final observation, that will be encountered again when reconstructing the top mass and when plotting jet profiles, is the significantly larger number of surviving events for $\alpha_S = 0.1200$ compared to $\alpha_S = 0.1500$. That is, of course, entirely reasonable since, as we shall see later, ISR and FSR effects create a significant background noise. Thus, the lower the value of the coupling is, the closer we get to the perfect situation of no extra radiation, as in Fig. 1.

- **Reconstructed top quark mass** ($p_\perp > 25\,\text{GeV}$, $|\eta| < 2.5$, $n_{\text{jet}} \geq 4$, $n_b = 2$, $60\,\text{GeV} \leq m_W \leq 90\,\text{GeV}$)

  The mass of the top quark is reconstructed with the successful events, which are estimated to be approximately 11% of the initial ones. The invariant mass of the W is added to the invariant mass of one of the b-jets. The problem is, however, that we do not know which is the b-jet that originated from the same top quark as the hadronically decayed boson. To solve this, the four-momentum of the W is added to both b-jets. The value that is closer to the *true* top mass (the default PYTHIA value, $m_t = 171.00\,\text{GeV}$) is considered the correct mass.

  Three different limits have been set (Fig. 4f, 4g and 4h), where the first one is the broadest and includes the tails of the distribution. With the second limitation, the plot is cut almost symmetrically, having the peaks in the center, whereas the last cut is the most fine and precise one. Top quark masses obtained from these three sets of histograms are shown in the last three rows of Table 1. Just as for the W mass, the numbers in the table show a negative shift (towards lower values) as we increase the coupling constant. The effect is rather small and this conclusion cannot be deduced by simply looking at the histograms. As before, we also note the difference in the area of the three histograms.

Table 1: The number of surviving events after each cut for the three different α_S values, where the second coupling is PYTHIA's default value. The last row shows what percentage of the total number of events has survived the very last cut.

	Cuts \ α_S	$\alpha_S = 0.1200$	$\alpha_S = 0.1365$	$\alpha_S = 0.1500$
1.	Start	2,000,000	2,000,000	2,000,000
2.	Lepton $p_\perp > 25\,\text{GeV}$	1,500,453	1,498,850	1,498,972
3.	Lepton $\eta < 2.5$	1,447,017	1,445,355	1,446,117
4.	Jet Multiplicity ≥ 4	820,518	835,143	842,725
5.	b-Jet Multiplicity $= 2$	527,930	517,608	507,120
6.	$0\,\text{GeV} \leq m_W \leq 160\,\text{GeV}$	418,354	403,935	390,732
7.	$60\,\text{GeV} \leq m_W \leq 90\,\text{GeV}$	248,760	228,147	213,100
8.	$100\,\text{GeV} \leq m_t \leq 300\,\text{GeV}$	247,528	226,810	211,644
9.	$130\,\text{GeV} \leq m_t \leq 200\,\text{GeV}$	230,602	209,164	193,985
10.	$150\,\text{GeV} \leq m_t \leq 180\,\text{GeV}$	174,660	153,605	139,049
11.		8.73%	7.68%	6.95%

Table 2: For the imposed cuts in rows from 6. to 10. in Table 1, the mean values of the masses of the W-boson and the top quark are given in GeV. The large difference in values from the respective cuts is owed to the asymmetric nature of the smeared Breit-Wigners and of the cuts, as can be seen on Figs. 4e and 4f. The final cuts are chosen such that the peaks of the histograms lie approximately at the center of the chosen region.

Cuts \ α_S	$\alpha_S = 0.1200$	$\alpha_S = 0.1365$	$\alpha_S = 0.1500$
$0\,\text{GeV} \leq m_W \leq 160\,\text{GeV}$	83.56 ± 0.04	83.90 ± 0.04	83.97 ± 0.05
$60\,\text{GeV} \leq m_W \leq 90\,\text{GeV}$	75.88 ± 0.01	75.48 ± 0.01	75.14 ± 0.02
$100\,\text{GeV} \leq m_t \leq 300\,\text{GeV}$	163.83 ± 0.04	163.67 ± 0.04	163.69 ± 0.05
$130\,\text{GeV} \leq m_t \leq 200\,\text{GeV}$	162.65 ± 0.03	162.33 ± 0.03	162.15 ± 0.03
$150\,\text{GeV} \leq m_t \leq 180\,\text{GeV}$	164.22 ± 0.02	164.00 ± 0.02	163.79 ± 0.02

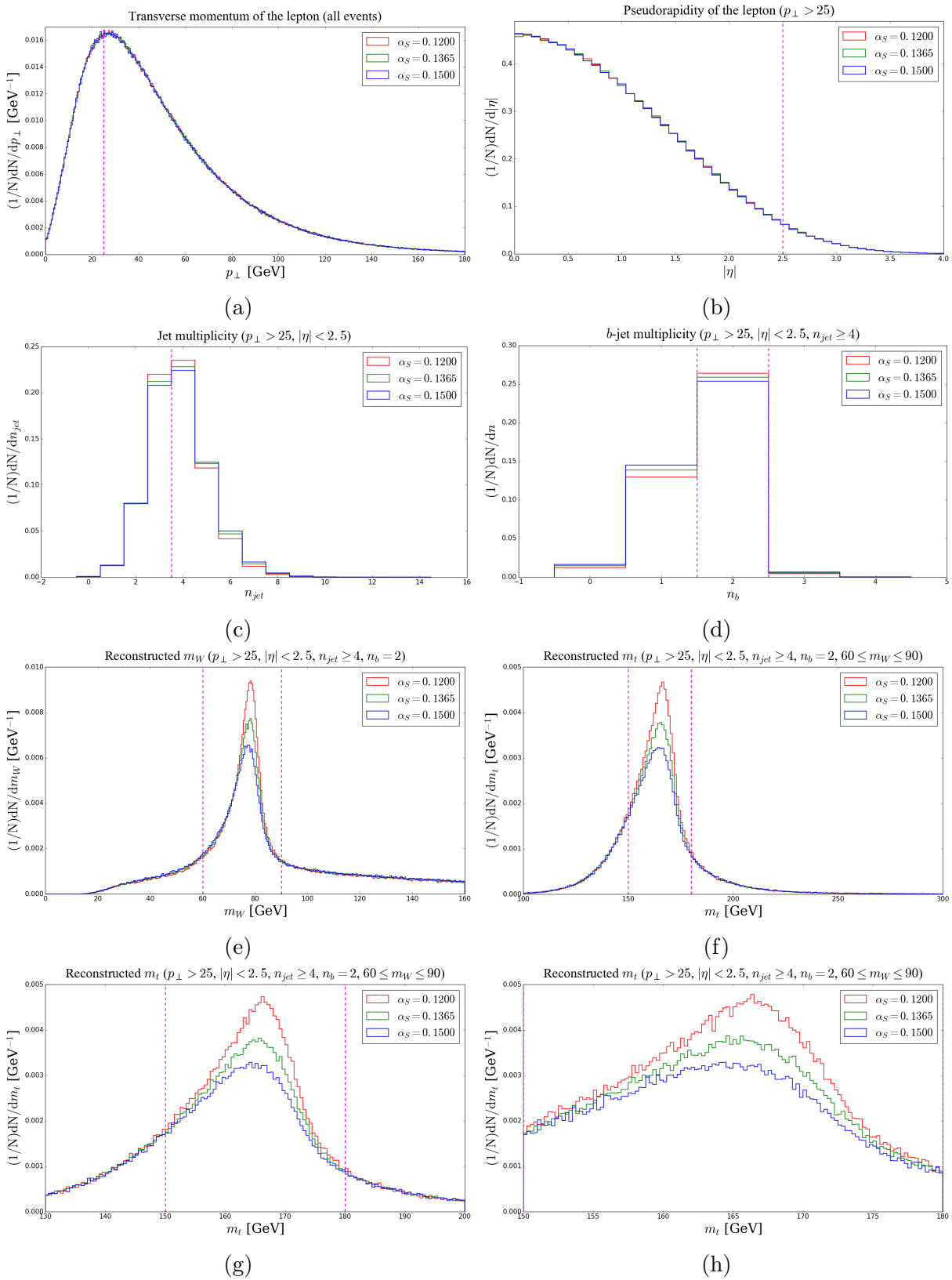

Figure 4: The plots representing the flow of the program. A magenta dashed line indicates the border between events that survive the respective cut and the ones that are not considered further.

5.2 Jet Profiles

The mass of the top is reconstructed by taking the four-momentum sum of three selected jets in an event. We shall therefore study the dynamics within these jets in order to evaluate the impact that parton showers have on them. As discussed in [4], the shift in the top mass can originate either from changes in the four-momentum, or changes in the radial separation between jets. In this project it is concentrated on the former issue, which is studied with the help of jet profile plots. They are produced for all hard $2 \to 2$ QCD processes and the results for the three α_S values are superimposed. To have overall $p_\perp$ scales comparable with top events, a $p_\perp > 200\,\text{GeV}$ is imposed. The differential jet shape is of the form:

$$\rho(r) = \frac{1}{N_{\text{jets}}} \sum_{j \in \text{jets}} \frac{\sum_{i \in \text{finalState}} p_{\perp i}(r_i)}{p_{\perp j}} \tag{27}$$

The transverse momentum of a single jet, $p_{\perp j}$, is calculated as the sum of the transverse momenta of all particles that constitute the jet. Then, the $p_\perp$ of all final-state particles inside the jet (or the whole event) are divided by the aforementioned momentum. This is summed over all jets in all events and finally normalized by their number. The quantity $\rho(r)$ then gives us the transverse momentum distribution over a distance r.

In order to study the relative difference between the various algorithms, we choose one according to which the rest of the alternatives are tuned — in this case, the default Pythia shower. Ideally, one would of course use experimental data. For comparison with the tuned data, all showers are also run with the default strong coupling, $\alpha_S = 0.1365$. The list below describes each of the studied jet profile plots on Fig. 5.

a) The first jet profile considers the $p_\perp$ of all jet constituents. Below the graph, the difference between the non-default histograms and the default Pythia one is plotted, following the same color-coding for the respective values. Since the radius of the jet cone is $R = 0.4$, there is no momentum distributed at distances larger than this value. An expected result (also described in [4]) is the difference in jet broadening for the three strong coupling values. We see that for $\alpha_S = 0.1200$, the concentration of high momentum in the center of the jet is bigger, whereas it spreads more and more as the parameter is increased. The stronger radiation results in the possible spread of decay products outside the radius of the jet cone. As a consequence, the reconstructed top mass for $\alpha_S = 0.1500$ is slightly less (almost half a GeV) than that for $\alpha_S = 0.1200$, as we have seen.

b) The two following graphs study the constituents of the jet, as in a). However, jets are considered separately depending on their transverse momentum. It is clearly seen how much narrower the high-$p_\perp$ jet profile is, compared with the low-$p_\perp$ one.

c) The last distribution is the normalized jet multiplicity of the events. As discussed previously, larger coupling values favour the production of more jets.

For the rest of the studies in Secs. 5.4, 5.5 and 5.6, we will only show the plots described in a) and c).

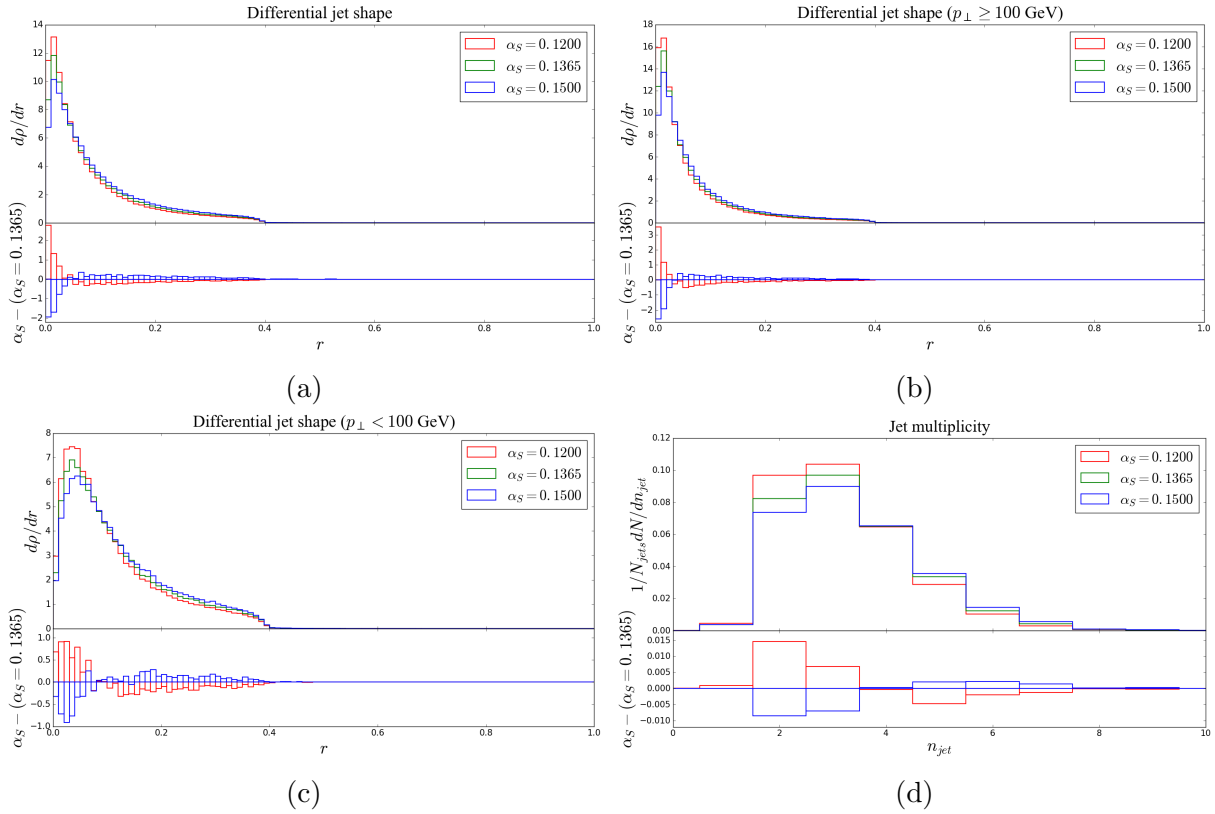

Figure 5: Jet profile of hard QCD events using PYTHIA. The plots are done for three different α_S values. The lower part of each plot gives the difference between the histograms of the alternatives and the histogram of the default PYTHIA value (green line), keeping the corresponding colors.

5.3 FSR, ISR and MPI Studies in Pythia

It is interesting to compare the behaviour of the events once either both ISR and FSR are completely switched off, or MPI is turned off, or neither of the three effects is present. This is done only for the case where α_S takes its default value of 0.1365 and the results are presented in Table 3 and Fig. 6.

The most noticeable difference is the area below the curves. The absence of ISR and FSR plays a significant role in the number of events that satisfy all cuts. Also MPI has a noticeable impact, but not as big. We can also notice the negative shift in the histograms when MPI is turned off. This is due to the fact that collisions between other proton constituents are then not taken into consideration. This results in a lower underlying-event particle multiplicity, and consequently fewer particles contribute to the mass reconstruction. From the table it is seen that the sharper peaks also lead to much smaller error in the results.

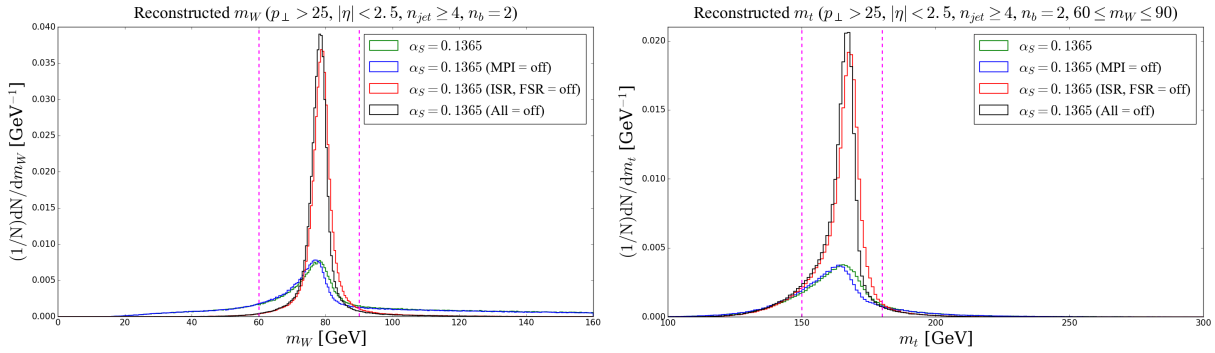

(a) (b)

Figure 6: The reconstructed W and top masses for the default PYTHIA α_S value where all effects are present (green line), where MPI is turned off (blue line), where ISR and FSR are turned off (red line) and where both radiation and MPI are off (black line). The magenta dashed line indicates the border between events that survive the respective cut and the ones that are not considered further.

Table 3: The reconstructed masses of the W-boson and the top quark are given in the cases where all effects are present, only ISR and FSR radiation is on, only MPI is on and finally, where no radiation and MPI affects the results.

Mode / Cuts	All = on	MPI = off	ISR, FSR = off	All = off
$0\,\text{GeV} \leq m_W \leq 160\,\text{GeV}$	83.90 ± 0.04	82.94 ± 0.05	79.14 ± 0.01	78.21 ± 0.01
$100\,\text{GeV} \leq m_t \leq 300\,\text{GeV}$	163.67 ± 0.04	162.38 ± 0.04	164.63 ± 0.02	163.37 ± 0.02
$130\,\text{GeV} \leq m_t \leq 200\,\text{GeV}$	162.33 ± 0.03	161.07 ± 0.03	164.67 ± 0.01	163.43 ± 0.01
$150\,\text{GeV} \leq m_t \leq 180\,\text{GeV}$	164.00 ± 0.02	162.94 ± 0.02	165.89 ± 0.01	164.78 ± 0.01

5.4 Dipole Recoil Effects in Pythia

The results are shown in Table 4 and Figs. 7, 8a, 8b. Here we study the dipole recoil algorithm option implemented in PYTHIA for ISR, where a single colour-connected final-state parton can take the recoil of an ISR emission. We notice that the two histograms with default strong coupling overlap almost perfectly. Nevertheless, this method slightly underestimates the masses of the W and the top in both cases with respect to the default PYTHIA shower. Resulting from the higher value of the coupling, the tuned α_S gives a lower number of surviving events.

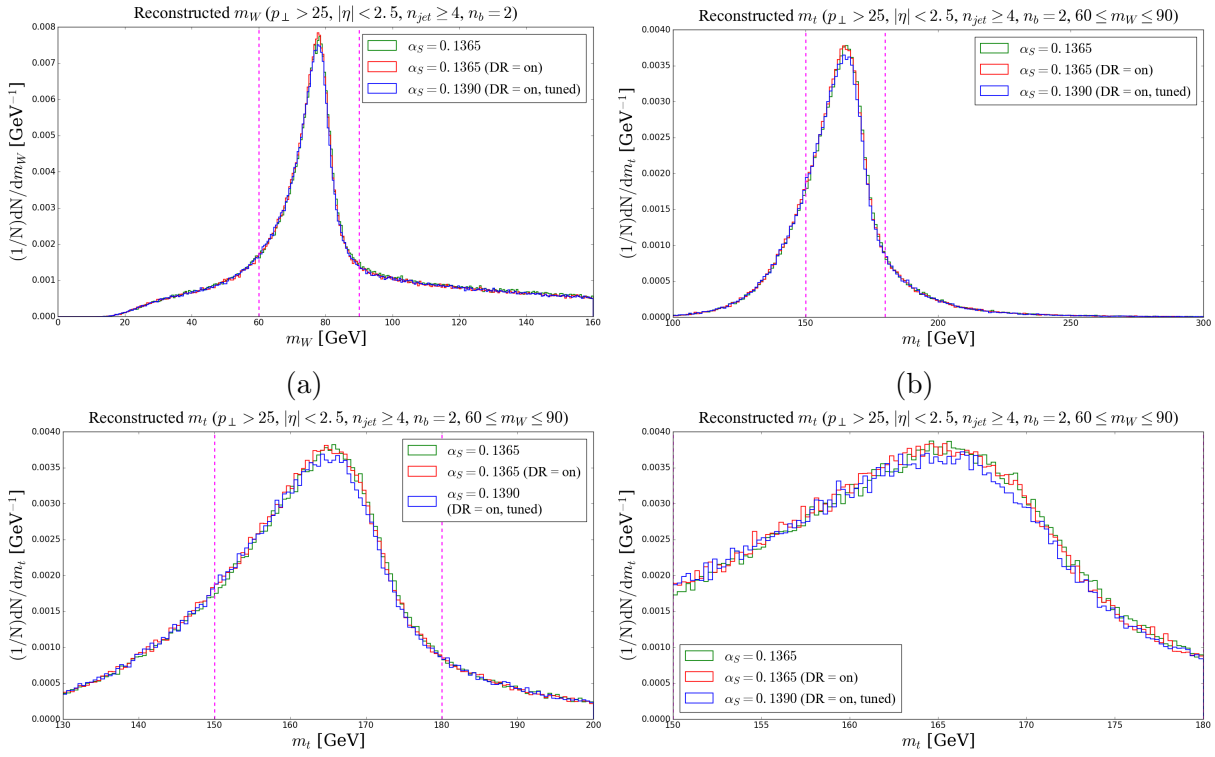

Figure 7: The reconstructed W and top masses for the default PYTHIA α_S value (green line), the default value with dipole recoil (DR) on (red line) and the tuned value with DR on (blue line). The magenta dashed line indicates the border between events that survive the respective cut and the ones that are not considered further.

Table 4: For the imposed cuts in rows from 6. to 10. in Table 1, the mean values of the masses of the W-boson and the top quark are given in GeV. As well as for the default PYTHIA settings, they are also evaluated when dipole recoil (DR) is turned on.

Cuts \ α_S	$\alpha_S = 0.1365$	$\alpha_S = 0.1365$ (DR = on)	$\alpha_S = 0.1390$ (DR = on, tuned)
$0\,\text{GeV} \leq m_W \leq 160\,\text{GeV}$	83.90 ± 0.04	83.41 ± 0.04	83.46 ± 0.04
$60\,\text{GeV} \leq m_W \leq 90\,\text{GeV}$	75.48 ± 0.01	75.36 ± 0.01	75.28 ± 0.01
$100\,\text{GeV} \leq m_t \leq 300\,\text{GeV}$	163.67 ± 0.04	163.36 ± 0.04	163.25 ± 0.04
$130\,\text{GeV} \leq m_t \leq 200\,\text{GeV}$	162.33 ± 0.03	162.11 ± 0.03	162.04 ± 0.03
$150\,\text{GeV} \leq m_t \leq 180\,\text{GeV}$	164.00 ± 0.02	163.85 ± 0.02	163.76 ± 0.02

Table 5: For the imposed cuts in rows from 6. to 10. in Table 1, the mean values of the masses of the W-boson and the top quark are given in GeV. The default PYTHIA α_S value has been used in DIRE (2nd column with results) and the masses from the tuned value are given in column 3.

Cuts \ α_S	$\alpha_S = 0.1365$	$\alpha_S = 0.1365$ (DIRE)	$\alpha_S = 0.1240$ (DIRE, tuned)
$0\,\text{GeV} \leq m_W \leq 160\,\text{GeV}$	83.90 ± 0.04	76.57 ± 0.03	77.15 ± 0.03
$60\,\text{GeV} \leq m_W \leq 90\,\text{GeV}$	75.48 ± 0.01	74.92 ± 0.01	75.55 ± 0.01
$100\,\text{GeV} \leq m_t \leq 300\,\text{GeV}$	163.67 ± 0.04	163.78 ± 0.03	164.12 ± 0.03
$130\,\text{GeV} \leq m_t \leq 200\,\text{GeV}$	162.33 ± 0.03	163.31 ± 0.02	163.65 ± 0.02
$150\,\text{GeV} \leq m_t \leq 180\,\text{GeV}$	164.00 ± 0.02	164.82 ± 0.01	165.08 ± 0.01

Table 6: For the imposed cuts in rows from 6. to 10. in Table 1, the mean values of the masses of the W-boson and the top quark are given in GeV. The default PYTHIA α_S value has been used in VINCIA (2nd column with results) and the masses from the tuned value are given in column 3.

Cuts \ α_S	$\alpha_S = 0.1365$	$\alpha_S = 0.1365$ (VINCIA)	$\alpha_S = 0.1300$ (VINCIA, tuned)
$0\,\text{GeV} \leq m_W \leq 160\,\text{GeV}$	83.90 ± 0.04	84.35 ± 0.05	84.21 ± 0.05
$60\,\text{GeV} \leq m_W \leq 90\,\text{GeV}$	75.48 ± 0.01	75.70 ± 0.02	75.86 ± 0.01
$100\,\text{GeV} \leq m_t \leq 300\,\text{GeV}$	163.67 ± 0.04	165.23 ± 0.05	165.14 ± 0.04
$130\,\text{GeV} \leq m_t \leq 200\,\text{GeV}$	162.33 ± 0.03	163.09 ± 0.03	163.11 ± 0.03
$150\,\text{GeV} \leq m_t \leq 180\,\text{GeV}$	164.00 ± 0.02	164.36 ± 0.02	164.43 ± 0.02

5.5 Pythia and Dire Showers

Results from the comparison between the PYTHIA and DIRE showers is given in Table 5 and Figs. 9, 8c, 8d. Since the events in DIRE usually have a weight different from unity, we have provided two plots of the weight distribution histogram, differing in their boundaries.

We can notice the different behaviour of the DIRE shower with respect to PYTHIA. Difference is noticed as early as the jet formation, where DIRE favours three-jet reconstruction. Therefore, only as many as 43% survive the $n_{\text{jet}} \geq 4$ cut compared to 57% in PYTHIA (for $\alpha_S = 0.1365$). This is greatly compensated for with the next cut, where $\approx 83\%$ of the surviving events in DIRE have a b-jet multiplicity of 2 in comparison with

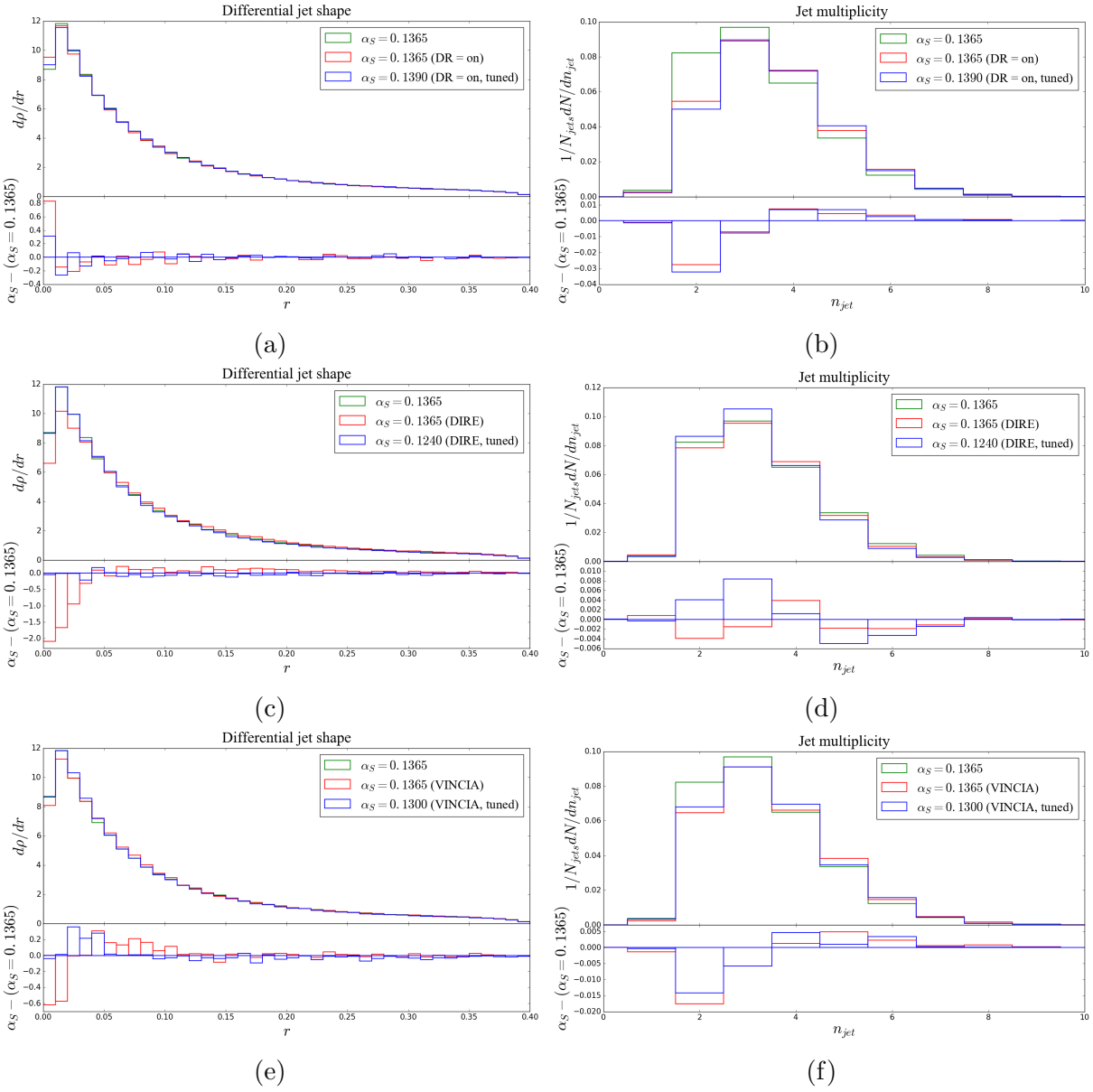

Figure 8: Jet profiles and jet multiplicities for hard $2 \to 2$ QCD events comparing the default Pythia shower with the dipole recoil (DR) option for ISR (a and b), with the dipole-like Dire algorithm (c and d) and the antenna-based Vincia algorithm (e and f).

62% in Pythia. From there, the reconstruction of the W and top masses results in a larger number of surviving events. In addition to the much sharper and higher mass peaks it is noticeable that Dire gives about a GeV higher average top mass.

As seen on Figs. 9e and 9f, event weights come with different signs. Additional care should then be taken when estimating error bars. More specifically, one could have split the run into multiple subruns, and made use of the spread of top masses between them.

Unfortunately, the long runs and the short project time did not permit to conduct such thorough estimations. Therefore, the usual method of uncertainty measures has been applied and presented in Table 5, namely take the ratio between the root-mean-square width of the data and the square root of the number of events that enter, but be cautioned that this is likely to be an underestimate by some factor.

5.6 Pythia and Vincia Showers

Lastly, we compare the reconstructed masses from PYTHIA and VINCIA. The results are shown in Table 6 and Figs.10, 8e, 8f. The surviving events from the latter are slightly less than the PYTHIA ones when run with $\alpha_S = 0.1365$. The tuned VINCIA shower overlaps almost perfectly with the default PYTHIA shower, having a slight positive shift of roughly 0.4 GeV higher top mass. The smaller (tuned) coupling value expectedly results in more surviving events. It should be noted that VINCIA rejected 7 and 4 bad events, respectively, out of 2 million ones in the normal and tuned runs. Nevertheless, the events surviving the last cut are 144, 132 and 151, 586 for the two runs, respectively, which is well below 153, 605 for the PYTHIA run (Table 1, row 10). The VINCIA CMW option [43] has been turned off for both the default and the tuned couplings. In these two cases, the running order of the coupling has been set to 1-loop, where the default option of the algorithm is 2-loop order corrections.

6 Conclusion

This report has given a brief introduction of the theory behind Monte Carlo event generators. Three different shower algorithms were used in our study, namely PYTHIA, DIRE and VINCIA. The reconstruction of the W-boson and top quark masses was performed with all three showers, thereby comparing their behaviour. What was eventually found in the study is a somewhat troublesome spread of results, amounting to approximately ± 0.5 GeV — a number that has been cited as the total uncertainty in the top mass by experimental collaborators.

A couple of important notes should be added. Firstly, the DIRE and VINCIA algorithms offer many more sophisticated treatments not taken into account in the runs. Secondly, the number of events surviving the very last cut differ for the three cases. The most significant difference compared to the rest of the showers was observed in DIRE, which predicted a much higher top mass peak. Moreover, a thorough study of the rest of the processes for all algorithms should be made, especially jet formation and b-jet behaviour, where significant differences in multiplicities have been observed.

As a final word, the findings from the thesis can be summed up in the following way. The experimental extraction of the top mass relies heavily on Monte Carlo event generators. Therefore, various shower algorithms are implemented in the attempt to asses theoretical uncertainties. It is important that the differences in their results are within the limits of the total experimental uncertainty — a requirement that was not confirmed by the

simulations. This points towards the need for more detailed and sophisticated studies, where event generation includes many other processes occurring in a collision, as well as use the algorithms up to their full potential.

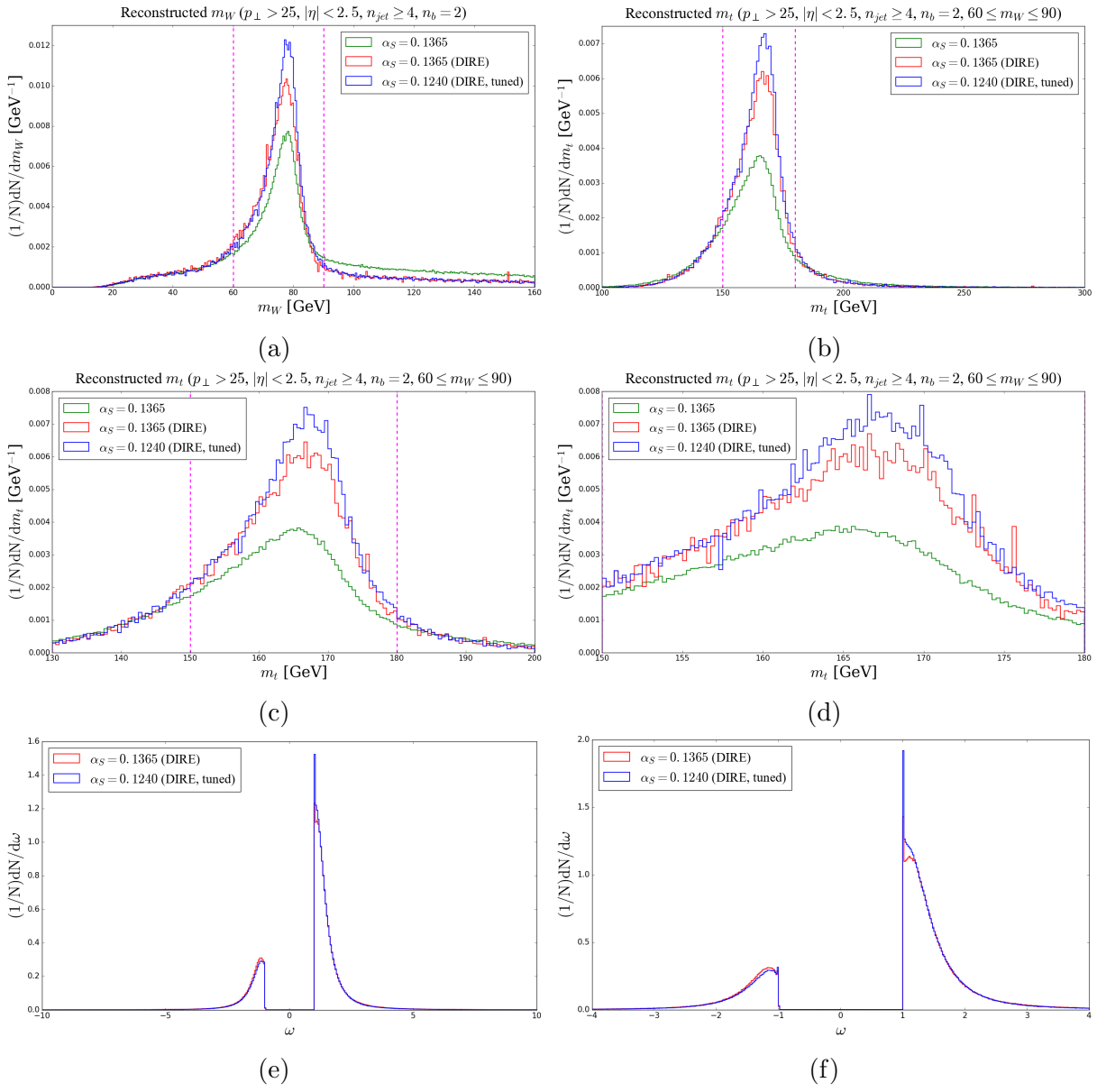

Figure 9: The reconstructed W and top masses for the default PYTHIA α_S value (green line), the default DIRE value (red line) and the tuned DIRE value (blue line). The magenta dashed line indicates the border between events that survive the respective cut and the ones that are not considered further. The two final subfigures give the weight distribution of the events.

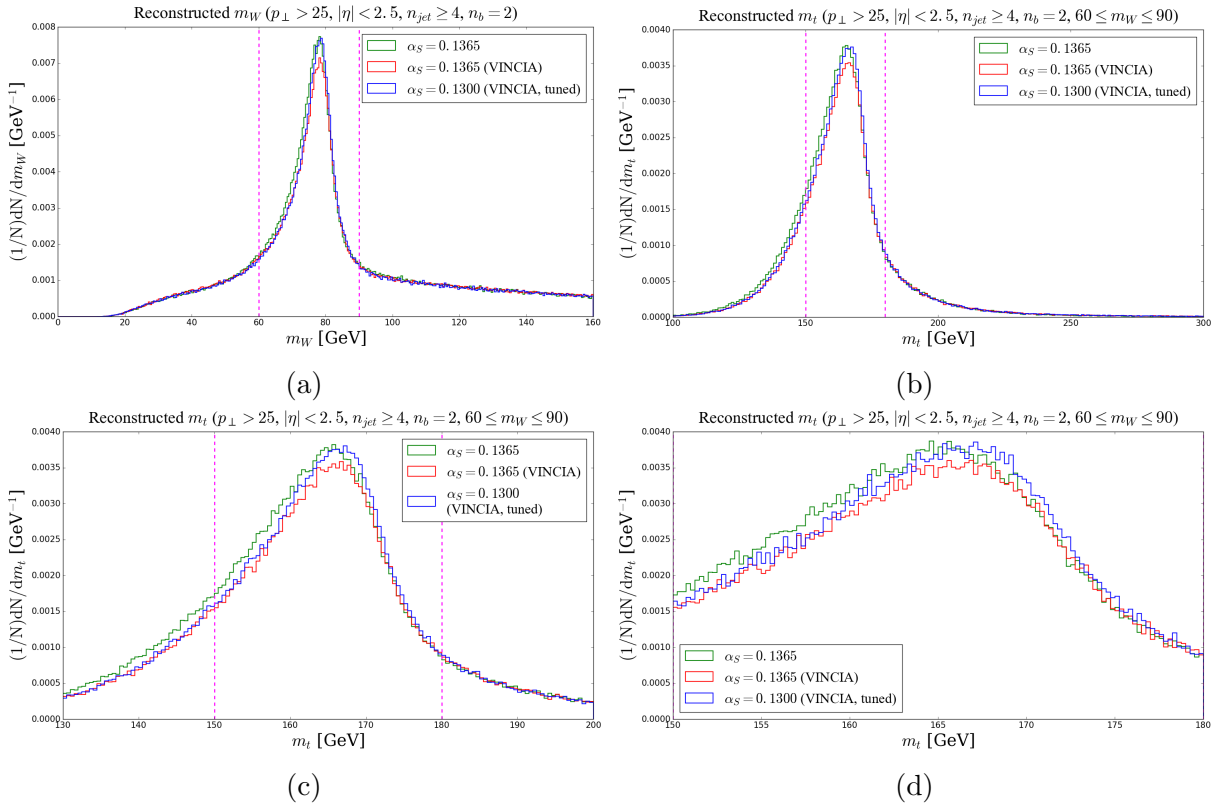

Figure 10: The reconstructed W and top masses for the default PYTHIA α_S value (green line), the default VINCIA value (red line) and the tuned VINCIA value (blue line). The magenta dashed line indicates the border between events that survive the respective cut and the ones that are not considered further.

Acknowledgements

I would like to express my sincere gratitude towards Torbjörn Sjöstrand for his incredible guidance, support and punctuality throughout the whole time. I am thankful for all his patience and the time he took to explain every single detail of the project, making sure I always understood it. It has been a pleasure!

I am also greatly thankful to Stefan Prestel for taking the time to discuss the details concerning the DIRE shower algorithm and Peter Skands of the School of Physics and Astronomy at the Monash University for sending us the VINCIA program and giving a feedback on the text regarding the algorithm — the analysis would not have been complete without it.

Finally, I would like to thank my family for their endless help and support!

References

[1] T. Ohl, "Drawing Feynman diagrams with Latex and Metafont," *Comput. Phys. Commun.* **90** (1995) 340–354 IKDA-95-20, arXiv:hep-ph/9505351 [hep-ph].

[2] F. Bezrukov and M. Shaposhnikov, "Why should we care about the top quark Yukawa coupling?," *J. Exp. Theor. Phys.* **120** (2015) 335–343 CERN-PH-TH-2014-218, arXiv:1411.1923 [hep-ph]. [Zh. Eksp. Teor. Fiz.147,389(2015)].

[3] T. Sjöstrand, S. Mrenna, and P. Z. Skands, "PYTHIA 6.4 Physics and Manual," *JHEP* **05** (2006) 026 FERMILAB-PUB-06-052-CD-T, LU-TP-06-13, arXiv:hep-ph/0603175 [hep-ph].

[4] S. Argyropoulos and T. Sjöstrand, "Effects of color reconnection on $t\bar{t}$ final states at the LHC," *JHEP* **11** (2014) 043, arXiv:1407.6653 [hep-ph].

[5] T. Sjöstrand and M. van Zijl, "A Multiple Interaction Model for the Event Structure in Hadron Collisions," *Phys. Rev.* **D36** (1987) 2019 LU-TP-87-5.

[6] T. Sjöstrand, "Colour reconnection and its effects on precise measurements at the LHC," LU-TP-13-37, MCNET-13-16, arXiv:1310.8073 [hep-ph].

[7] T. Sjöstrand, S. Ask, J. R. Christiansen, R. Corke, N. Desai, P. Ilten, S. Mrenna, S. Prestel, C. O. Rasmussen, and P. Z. Skands, "An Introduction to PYTHIA 8.2," *Comput. Phys. Commun.* **191** (2015) 159–177 LU-TP-14-36, MCNET-14-22, CERN-PH-TH-2014-190, FERMILAB-PUB-14-316-CD, DESY-14-178, SLAC-PUB-16122, arXiv:1410.3012 [hep-ph].

[8] T. Sjöstrand and P. Z. Skands, "Transverse-momentum-ordered showers and interleaved multiple interactions," *Eur. Phys. J.* **C39** (2005) 129–154 LU-TP-04-29, arXiv:hep-ph/0408302 [hep-ph].

[9] S. Höche and S. Prestel, "The midpoint between dipole and parton showers," *Eur. Phys. J.* **C75** no. 9, (2015) 461 SLAC-PUB-16304, MCNET-15-13, arXiv:1506.05057 [hep-ph].

[10] S. Höche and S. Prestel, "Triple collinear emissions in parton showers," *Phys. Rev.* **D96** no. 7, (2017) 074017 SLAC-PUB-16963, FERMILAB-PUB-17-122-T, MCNET-17-05, arXiv:1705.00742 [hep-ph].

[11] S. Höche, F. Krauss, and S. Prestel, "Implementing NLO DGLAP evolution in Parton Showers," *JHEP* **10** (2017) 093 SLAC-PUB-16965, FERMILAB-PUB-17-134-T, IPPP-17-34, DCPT-17-68, MCNET-17-06, arXiv:1705.00982 [hep-ph].

[12] N. Fischer, S. Prestel, M. Ritzmann, and P. Skands, "Vincia for Hadron Colliders," *Eur. Phys. J.* **C76** no. 11, (2016) 589 COEPP-MN-16-11, MCNET-16-13, SLAC-PUB-16529, NIKHEF-2016-020, arXiv:1605.06142 [hep-ph].

[13] P. Bärnreuther, M. Czakon, and A. Mitov, "Percent Level Precision Physics at the Tevatron: First Genuine NNLO QCD Corrections to $q\bar{q} \to t\bar{t} + X$," *Phys. Rev. Lett.* **109** (2012) 132001 CERN-PH-TH-2012-092, arXiv:1204.5201 [hep-ph].

[14] M. Czakon and A. Mitov, "NNLO corrections to top pair production at hadron colliders: the quark-gluon reaction," *JHEP* **01** (2013) 080 CERN-PH-TH-2012-286, arXiv:1210.6832 [hep-ph].

[15] M. Czakon, P. Fiedler, and A. Mitov, "Total Top-Quark Pair-Production Cross Section at Hadron Colliders Through $O(\frac{4}{S})$," *Phys. Rev. Lett.* **110** (2013) 252004 CERN-PH-TH-2013-056, TTK-13-08, arXiv:1303.6254 [hep-ph].

[16] B. Cabouat, "Parton shower algorithms - possible improvements," 2017. http://lup.lub.lu.se/student-papers/record/8914885. Student Paper.

[17] T. Sjöstrand, "Monte Carlo Tools," in *Proceedings, 65th Scottish Universities Summer School in Physics: LHC Physics (SUSSP65): St. Andrews, UK, August 16-29, 2009*, pp. 309–339. 2009. arXiv:0911.5286 [hep-ph].

[18] B. Cabouat and T. Sjöstrand, "Some Dipole Shower Studies," *Eur. Phys. J.* **C78** no. 3, (2018) 226 MCNET-17-14, LU-TP-17-28, arXiv:1710.00391 [hep-ph].

[19] G. Altarelli and G. Parisi, "Asymptotic Freedom in Parton Language," *Nucl. Phys.* **B126** (1977) 298–318 LPTENS-77-6.

[20] J. Campbell, J. Huston, and F. Krauss, *The Black Book of Quantum Chromodynamics*. Oxford University Press, 2017. https://global.oup.com/academic/product/the-black-book-of-quantum-chromodynamics-9780199652747.

[21] T. Sjöstrand, "A model for initial state parton showers," *Physics Letters B* **157** no. 4, (1985) 321 – 325. http://www.sciencedirect.com/science/article/pii/0370269385906744.

[22] G. Gustafson, "Dual Description of a Confined Color Field," *Phys. Lett.* **B175** (1986) 453 LU TP 86-5. [,193(1986)].

[23] G. Gustafson and U. Pettersson, "Dipole Formulation of QCD Cascades," *Nucl. Phys.* **B306** (1988) 746–758 LU-TP-87-9.

[24] G. 't Hooft, "A Planar Diagram Theory for Strong Interactions," *Nucl. Phys.* **B72** (1974) 461 CERN-TH-1786. [,337(1973)].

[25] L. Lönnblad, "ARIADNE version 4: A Program for simulation of QCD cascades implementing the color dipole model," *Comput. Phys. Commun.* **71** (1992) 15–31 DESY-92-046.

[26] S. Höche, F. Krauss, M. Schönherr, and F. Siegert, "A critical appraisal of NLO+PS matching methods," *JHEP* **09** (2012) 049 SLAC-PUB-14661, IPPP-11-67, DCPT-11-134, LPN11-58, FR-PHENO-2011-019, MCNET-11-24, arXiv:1111.1220 [hep-ph].

[27] S. Plätzer and M. Sjödahl, "The Sudakov Veto Algorithm Reloaded," *Eur. Phys. J. Plus* **127** (2012) 26 DESY-11-146, KA-TP-22-2011, MCNET-11-19, arXiv:1108.6180 [hep-ph].

[28] L. Lönnblad, "Fooling Around with the Sudakov Veto Algorithm," *Eur. Phys. J.* **C73** no. 3, (2013) 2350 MCNET-12-16, LU-TP-12-44, arXiv:1211.7204 [hep-ph].

[29] W. T. Giele, D. A. Kosower, and P. Z. Skands, "Higher-Order Corrections to Timelike Jets," *Phys. Rev.* **D84** (2011) 054003 FERMILAB-PUB-10-515-T, CERN-PH-TH-2010-283, SACLAY-IPHT-T10-196, MCNET-11-05, arXiv:1102.2126 [hep-ph].

[30] T. Sjöstrand and P. Z. Skands, "Multiple interactions and the structure of beam remnants," *JHEP* **03** (2004) 053 LU-TP-04-08, arXiv:hep-ph/0402078 [hep-ph].

[31] B. R. Webber, "A QCD Model for Jet Fragmentation Including Soft Gluon Interference," *Nucl. Phys.* **B238** (1984) 492–528 CERN-TH-3713.

[32] B. Andersson, "The Lund model," *Camb. Monogr. Part. Phys. Nucl. Phys. Cosmol.* **7** (1997) 1–471.

[33] B. Andersson, G. Gustafson, G. Ingelman, and T. Sjöstrand, "Parton Fragmentation and String Dynamics," *Phys. Rept.* **97** (1983) 31–145 LU-TP-83-10.

[34] T. Sjöstrand, "The Lund Monte Carlo for Jet Fragmentation and e+ e- Physics: Jetset Version 6.2," *Comput. Phys. Commun.* **39** (1986) 347–407 LU-TP-85-10.

[35] T. Sjöstrand, "Jet Fragmentation of Nearby Partons," *Nucl. Phys.* **B248** (1984) 469–502 DESY-T-84-01.

[36] G. P. Salam, "Towards Jetography," *Eur. Phys. J.* **C67** (2010) 637–686, arXiv:0906.1833 [hep-ph].

[37] M. Cacciari, G. P. Salam, and G. Soyez, "The anti-k_t jet clustering algorithm," *JHEP* **04** (2008) 063 LPTHE-07-03, arXiv:0802.1189 [hep-ph].

[38] E. Gardi, N. Glover, and A. Robson, *LHC Phenomenology.* Springer, Cham, 2015.

[39] J. D. Hunter, "Matplotlib: A 2D Graphics Environment," *Comput. Sci. Eng.* **9** no. 3, (2007) 90–95.

[40] **ATLAS** Collaboration, T. A. collaboration, "Measurement of the Top Quark Mass from $\sqrt{s} = 7$ TeV ATLAS Data using a 3-dimensional Template Fit," ATLAS-CONF-2013-046.

[41] M. Thomson, *Modern Particle Physics.* Cambridge University Press, 2013.

[42] **Particle Data Group** Collaboration, C. Patrignani *et al.*, "Review of Particle Physics," *Chin. Phys.* **C40** no. 10, (2016) 100001.

[43] S. Catani, B. R. Webber, and G. Marchesini, "QCD coherent branching and semiinclusive processes at large x," *Nucl. Phys.* **B349** (1991) 635–654 CAVENDISH-HEP-90-11, UPRF-90-280.